Organic Sensitizers Based on Hexylthiophene-Functionalized Indolo[3,2-b]carbazole for Efficient Dye-Sensitized Solar Cells

ARTICLE *in* THE JOURNAL OF PHYSICAL CHEMISTRY C · JULY 2009

Impact Factor: 4.77 · DOI: 10.1021/jp808536v

6 AUTHORS, INCLUDING:

Zhong-Sheng Wang
Fudan University
107 PUBLICATIONS **7,306** CITATIONS
SEE PROFILE

Nagatoshi Koumura
National Institute of Advanced Industrial S…
76 PUBLICATIONS **4,221** CITATIONS
SEE PROFILE

Kohjiro Hara
National Institute of Advanced Industrial S…
154 PUBLICATIONS **11,267** CITATIONS
SEE PROFILE

Organic Sensitizers Based on Hexylthiophene-Functionalized Indolo[3,2-*b*]carbazole for Efficient Dye-Sensitized Solar Cells

Xue-Hua Zhang, Zhong-Sheng Wang, Yan Cui, Nagatoshi Koumura,* Akihiro Furube, and Kohjiro Hara*

National Institute of Advanced Industrial Science and Technology, 1-1-1 Higashi, Tsukuba, Ibaraki 305-8565, Japan

Received: September 26, 2008; Revised Manuscript Received: May 25, 2009

Two new organic sensitizers, **MKZ-21** and **MKZ-22**, comprising 5,11-dioctylindolo[3,2-*b*]carbazole moiety as the electron donor, *n*-hexyl-substituted oligothiophene units as the π-conjugated bridge, and cyanoacrylic acid group as the electron acceptor were designed and synthesized for application in dye-sensitized nanocrystalline TiO_2 solar cells (DSSCs). Theoretical calculation indicates that HOMO−LUMO excitation moves the electron distribution from the indolo[3,2,-*b*]carbazole moiety to the cyanoacrylic acid (cyanoacrylate) group. Compared with a sensitizer **MK-1** based on a carbazole unit as the electron donor, both experimental results and theoretical calculations prove that, when connected into the similar donor-π-acceptor structure, indolo[3,2-*b*]carbazole unit has stronger electron donating ability than the carbazole unit. For the functionalized organic sensitizers **MKZ-21** and **MKZ-22**, upon anchoring onto TiO_2 film, **MKZ-21** exhibited a better photovoltaic performance: a monochromatic incident photon-to-current conversion efficiency (IPCE) of 83%, a short-circuit photocurrent density (J_{sc}) of 15.4 mA cm^{-2}, an open-circuit voltage (V_{oc}) of 0.71 V, and a fill factor (FF) of 0.67, corresponding to an overall conversion efficiency (η) of 7.3% under standard AM 1.5G irradiation (100 mW cm^{-2}), which suggests that the sensitizers based on indolo[3,2,-*b*]carbazole unit are promising candidates for DSSCs.

Introduction

As low-cost alternatives to conventional solid-state photovoltaic devices, dye-sensitized solar cells (DSSCs) have attracted extensive interest following their discovery in 1991.[1] Sensitizers, as a crucial element (light harvesting component) in DSSCs, exert significant influence on the photovoltaic performance. Although ruthenium polypyridyl complexes[2−5] still represent the most efficient sensitizers so far, metal-free organic sensitizers have also been attracting intensive research efforts by virtue of their high molar extinction coefficients and facile modification, as well as environmentally friendly and inexpensive production techniques. Over the past decades, many kinds of metal-free organic sensitizers[6−20] have been extensively investigated for DSSC applications, and impressive photoelectric conversion efficiency value up to 9% under AM 1.5G irradiation has been achieved through appropriate molecular design.[13]

Indolo[3,2-*b*]carbazole derivatives[21−27] were demonstrated to possess excellent hole-transporting ability and have been used as the active layer in fields of organic light-emitting diodes and organic thin-film transistors. Compared with carbazole, indolo[3,2-*b*]carbazole unit presents a structure similar to pentacene, in terms of planarity, with addition of the two nitrogen atoms on which alkyl or alkyl chains can be added to enhance the solubility of the materials. As we have reported, carbazole derivatives can be used as efficient sensitizers for DSSCs,[14,19] we envisioned that indolo[3,2-*b*]carbazole unit could act as an efficient electron donor, and in the similar donor-π-acceptor structure, may have stronger electron donating ability, which could lead to red shift of absorption spectrum, than the carbazole unit. With appropriate π-conjugated bridge and appropriate electron acceptor and anchoring group, sensitizers based on indolo[3,2-*b*]carbazole unit would be interesting candidates for DSSCs. According to the above anticipation, we designed and synthesized a new class of organic sensitizers, 2-cyano-3-[3′,4-di-*n*-hexyl-5′-(5,11-dioctylindolo[3,2-*b*]carbazol-2-yl)-[2,2′]bithiophen-5-yl]acrylic acid (**MKZ-21**) and 2-cyano-3-[5″-(5,11-dioctylindolo[3,2-*b*]carbazol-2-yl)-3′,3″,4-tri-*n*-hexyl-[2,2′,5′,2″]terthiophen-5-yl]acrylic acid (**MKZ-22**), as shown in Figure 1, based on 5,11-dioctylindolo[3,2-*b*]carbazole moiety as a donor, *n*-hexyl-substituted oligothiophene units as a π-conjugation linkage, and cyanoacrylic acid as an acceptor and anchoring group, for DSSCs applications. The long *n*-octyl chains were chosen here to provide good solubility of the intermediates and the final sensitizers. The oligothiophene linkage was substituted by *n*-hexyl groups to suppress charge recombination, improve the open-circuit voltage, suppress the aggregation of the sensitizers, and hence to increase the solar-to-electric power conversion efficiency.[14,19] Finally, the hydrophobic long *n*-octyl and *n*-hexyl aliphatic chains could also enhance the long-term stability of the solar cell through preventing water induced dye desorption from the TiO_2 surface.[28−30]

In this study, we report on their synthesis, characterization, and photovoltaic properties, and compare them with a sensitizer **MK-1** (Figure S1),[14,19] which consists of similar π-conjugation linkage and the same acceptor/anchoring group, but using N-ethylcarbazole moiety as the electron donor. Moreover, we perform density functional theory (DFT) and time-depended density functional theory (TD-DFT) calculations to provide a detailed characterization of the structural, electronic, and optical properties of the two sensitizers. To the best of our knowledge, this is the first report on the performance of DSSCs based on indolo[3,2,-*b*]carbazole derivatives.

* Corresponding author. Phone: +81-29-861-4638. Fax: +81-29-861-4638. E-mail: n-koumura@aist.go.jp (N. K.) and k-hara@aist.go.jp (K. H.).

10.1021/jp808536v CCC: $40.75
Published on Web 07/02/2009

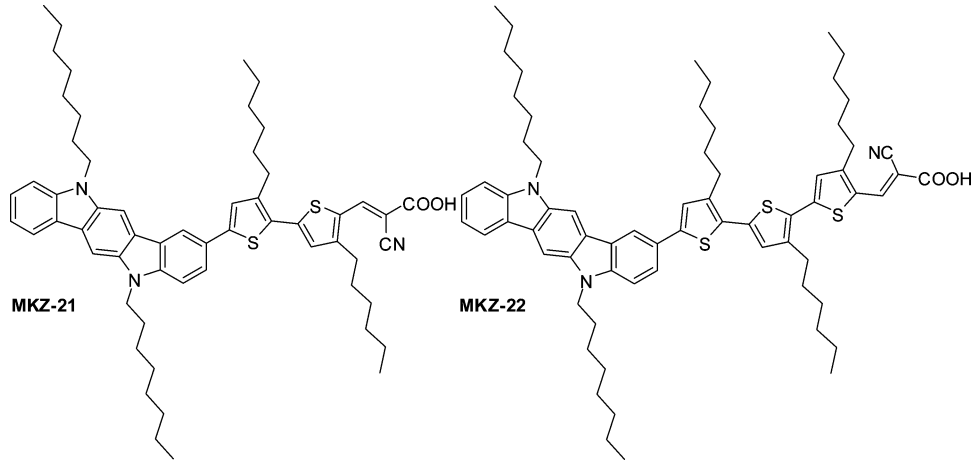

Figure 1. Molecular structures of **MKZ-21** and **MKZ-22**.

Experimental Section

General Procedure and Dye Synthesis. All starting materials and solvents for synthesis, measurements, and solar cell fabrication were purchased from Wako Chemicals, Kanto Chemicals, Tomiyama Pure Chemical Industries Ltd., Aldrich, Tokyo Chemical Industry Co., Ltd., and/or Merck and used without further purification. The sensitizers were synthesized using a modified procedure described in the previous literatures in moderate yields, and the synthetic route is illustrated in Supporting Information. Absorption spectra were measured on a SHIMADZU UV-3101 PC spectrophotometer, solvents used for spectroscopy experiments were spectrophotometric grade.

Electrochemical Measurements. Cyclic voltammetry measurements were carried out in a three-electrode electrochemical cell on a CHI610B electrochemical analyzer to determine the oxidation potentials of the sensitizers. Dye-loaded TiO_2 film, platinum, and Ag/Ag^+ were employed as working, counter, and reference electrodes, respectively. The supporting electrolyte was 0.1 M tetrabutylammonium perchlorate in acetonitrile and was degassed with N_2 for 20 min prior to scanning. The potential of the reference electrode is 0.49 V versus NHE and was calibrated with ferrocene immediately after CV measurements.

Molecular Orbital Calculation. Without any symmetry constraint in gas phase and by assuming the target molecules to be isolated, we optimized the molecular structure of the sensitizers, together with their lithium salts, on the Gaussian 03 program package[31] by using density functional theory (DFT). Lithium salt is the model for the sensitizer adsorbed on TiO_2 film. Becke's three-parameter hybrid functional with the LYP correlation functional (B3LYP) was employed together with 6-31G(d) basis set.[32] We further calculated the lowest singlet transitions of the sensitizers and also their lithium salts using time-depended density functional theory (TD-DFT) method.

Transient Absorption Spectroscopy. Ultrafast visible-pump/IR-probe femtosecond transient absorption spectroscopy was used to measure electron injection kinetics. Some details of our femtosecond transient absorption spectrometer have been described previously.[33] The light source for transient absorption spectroscopy was a femtosecond titanium sapphire laser with a regenerative amplifier (Hurricane, Spectra Physics, 800 nm, 150 fs, 1 mJ/pulse, 1 kHz). The fundamental output of the laser was divided into two beams. One of the beams was used for pump pulse at 525 nm, and another was used for probe pulse at 3440 nm. To obtain 525 nm light, an 800 nm beam was introduced into an optical parametric amplifier (OPA; TOPAS, Quantronix) with a mixing crystal. The IR (3440 nm) probe beam was obtained by introducing the 800 nm beam into another OPA (TOPAS, Quantronix) with a differential frequency generation crystal. The pump light entered the decay stage to change the pulse distance between pump and probe beams, thus achieving a time delay. A chopper was used to control pump-on and pump-off. The probe beam was divided into two beams: one beam passed through the sample, and another beam acted as a reference for compensating the intensity fluctuation of each pulse. The pump beam diameter on the film surface was about 0.4 mm, and its intensity was about 1 μJ. Signals from mercury−cadmium-telluride (MCT, Hamamatsu, P3257−10) photodetectors were gated and acquired. Transient absorption intensity was calculated from the pulse intensity of the probe with and without excitation, typically using thousands of pulses. The dye-sensitized film prepared on a glass substrate was covered by a thin glass substrate to hold electrolyte layer between the two glass substrates. The samples were scanned to minimize the effect of slight degradation of dyes during the experiments. All of the transient absorption measurements were performed at 295 K.

Preparation of Dye-Sensitized Nanocrystalline TiO_2 Solar Cells. F-SnO_2 (FTO) coated glass substrates were cleaned in a detergent solution by an ultrasonic bath, rinsed with water and ethanol, and then dried using N_2 current. Nanocrystalline TiO_2 electrodes, 6 μm (transparent layer, consisting of only ~20 nm nanoparticles) or 14 μm {consisting of a 9 μm transparent layer (~20 nm nanoparticles) and a 5 μm scattering layer [60% nanoparticles (~20 nm) and 40% large particles (~100 nm)]} in thickness were prepared using screen printing technique.[19] TiO_2 nanoparticles and an organic TiO_2 paste for screen printing were prepared according to the reported procedure.[34]

The dye adsorbed TiO_2 film electrode and Pt counter electrode were assembled into a sealed sandwich solar cell with a hot-melt Surlyn film (30 μm thickness) as spacer between the electrodes. A drop of the electrolyte solution was put on the drilled hole in the counter electrode of the assembled cell and was inhaled into the cell via the suction through another drilled hole. Finally, the two holes were sealed using additional hot-melt Surlyn film covered with a thin glass slide. In this work, three kinds of electrolytes were employed: electrolyte 1, 0.6 M 1,2-dimethyl-3-*n*-propylimidazolium iodide (DMPImI) + 0.1 M LiI + 0.05 M I_2 + 0.5 M 4-*tert*-butylpyridine (TBP) in acetonitrile (AN); electrolyte 2, 0.2 M instead of 0.05 M I_2 in

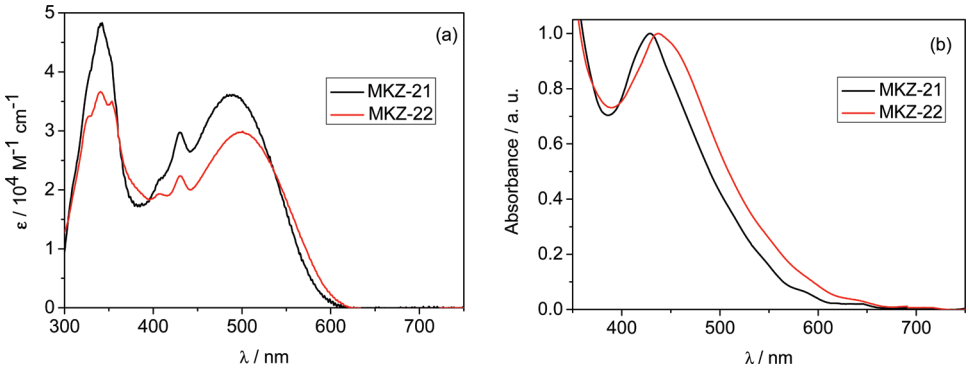

Figure 2. Absorption spectra of **MKZ-21** and **MKZ-22** in toluene solution (a) and on nanocrystalline TiO_2 film (b), using a bare TiO_2 film as a reference, obtained by soaking the film (transparent layer, ~20 nm nanoparticles, 1.5 μm in thickness) in a toluene solution containing 0.3 mM sensitizer overnight.

TABLE 1: Photophysical and Electrochemical Properties As Well As the Maximal Absorption on Nanocrystalline TiO_2 Film (Transparent Layer, ~20 nm Nanoparticles, 1.5 μm in Thickness) for MK-1, MKZ-21, and MKZ-22

sensitizer	λ_{max}/nm (ϵ/10^4 M^{-1} cm^{-1})	λ_{max}/nm (on TiO_2 film)	E_{ox}/V (vs NHE)	E_{0-0}/eV	E_{ox}*/V (vs NHE)
MK-1	492 (4.04)	428	1.07	2.00 (620 nm)	−0.93
MKZ-21	492 (3.60); 342 (4.81)	429	0.84	2.03 (610 nm)	−1.19
MKZ-22	501 (2.99); 341 (3.66)	437	0.93	1.85 (670 nm)	−0.92

[a] λ_{max} and the corresponding ϵ were obtained in toluene solution. E_{0-0} is derived from the absorption onset wavelength of the dye-loaded film.

electrolyte 1; electrolyte 3, replacing AN in electrolyte 1 with MPN (3-methoxypropionitrile).

Photovoltaic Measurements. The prepared dye-sensitized solar cells were illuminated through the conducting glass support with a black mask with an aperture area of 0.2354 cm^2 in order to avoid the penetrating of diffuse light into the active dye-loaded film (The apparent surface area of the TiO_2 film electrode was ca. 0.25 cm^2, 0.5 cm × 0.5 cm.). The performance of the dye sensitized solar cells was characterized by photocurrent action spectra and current−voltage measurements. Action spectra of the monochromatic incident photon-to-current conversion efficiency (IPCE) were measured with a CEP-99W system (Bunkoh-Keiki Co., Ltd.). The photocurrent−voltage (J−V) curves were obtained from a computer controlled source meter (Advantest, R6243) under illumination of simulated AM 1.5G solar light from an AM 1.5 solar simulator (Wacom Co., Japan, WXS80C-3 with a 300W Xe lamp and an AM 1.5 filter). The incident light intensity was calibrated by using a standard crystalline silicon solar cell with an IR-cutoff filter (Schott, KG-5), giving the photo response range of amorphous silicon solar cell produced and calibrated by Japan Quality Assurance Organization.

Results and Discussion

Absorption and Electrochemical Properties. Figure 2 shows the UV−vis spectra of the sensitizers **MKZ-21** and **MKZ-22** measured both in toluene solution and adsorbed on nanocrystalline TiO_2 film (transparent layer, ~20 nm nanoparticles, 1.5 μm in thickness). The corresponding absorption maxima, extinction coefficients at absorption maxima, and the absorption maxima on TiO_2 film are collected in Table 1. In toluene solution, both **MKZ-21** and **MKZ-22** exhibit two major prominent absorption bands, appearing at 310−360 nm and 450−560 nm, due to the π−π* transitions of the conjugated molecule. But owing to the deprotonation of the carboxylic acid, upon dye adsorption onto the TiO_2 surface,[3] the absorption spectra of **MKZ-21** and **MKZ-22** on TiO_2 films both exhibit blue shift, as shown in Figure 2b and Table 1. Both in solution and on TiO_2 surface, increasing the number of the thiophene units can make the absorption maximum of the sensitizer red-shifted (the λ_{max} values in solution and on TiO_2 surface are 492 and 429 nm for **MKZ-21**, respectively, as compared with 501 and 437 nm for **MKZ-22**) as a result of the extended π-conjugation, in keeping with our theoretical calculations presented below, making **MKZ-22** more efficient in long wave light harvesting. Under similar experimental conditions, we also measured the absorption spectra of **MK-1**; the data are listed in Table 1. The values of the absorption maxima of **MK-1** both in toluene solution and on TiO_2 film are similar to those of **MKZ-21**, but a little blue-shifted compared with those of **MKZ-22**, being consistent with the following calculated results, which indicates the stronger electron donating ability of indolo[3,2,-*b*]carbazole unit than that of carbazole unit.

The oxidation potentials of the two sensitizers were measured with cyclic voltammetry (Table 1), the excited state oxidation potentials (E_{ox}*) of **MKZ-21** and **MKZ-22** (**MKZ-21**, −1.19 V and **MKZ-22**, −0.92 V, versus NHE, normal hydrogen electrode) are much more negative than the conduction band edge of TiO_2, which is located at −0.5 V (vs NHE), and the ground state oxidation potentials (E_{ox}) (**MKZ-21**, 0.84 V and **MKZ-22**, 0.93 V, vs NHE) are sufficiently more positive than the iodine redox potential value (~0.4 V, vs NHE), thus providing a thermodynamic driving force for efficient electron injection and dye regeneration reaction.[35]

Theoretical Calculation. To get insight into the geometrical, electronic, and optical properties of these sensitizers, we optimized the geometries of the sensitizers, both in acid type and in their corresponding lithium salts, because the sensitizers are adsorbed onto the TiO_2 surface with carboxylate form, by Gaussian 03 program.[31] We first optimized their molecular structure in gas phase without any symmetry constraints; the optimized ground-state geometries and atom labeling are shown in Figure S2 (Supporting Information), while the main dihedral angles, by which the optimized geometries of the ground state

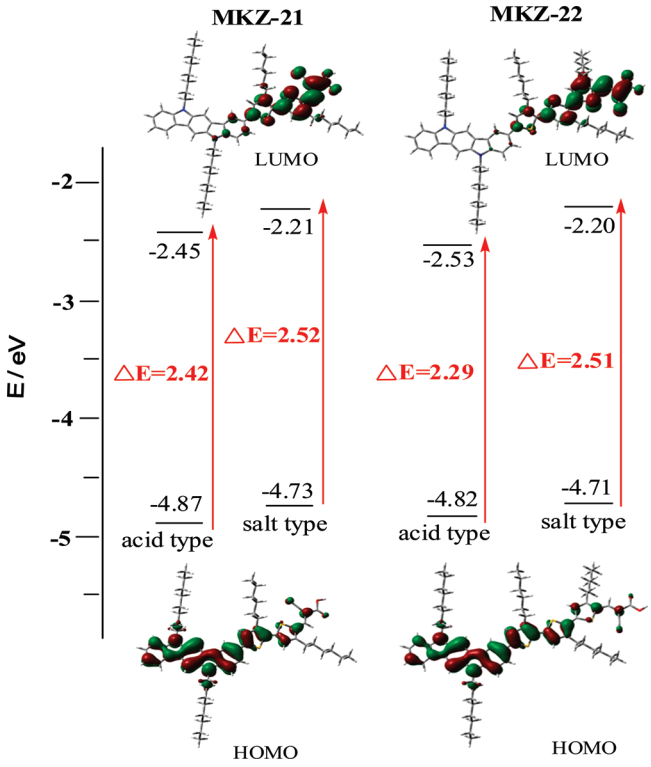

Figure 3. Calculated molecular orbital energy diagram and isodensity surface plots of the HOMOs and LUMOs for **MKZ-21** and **MKZ-22**.

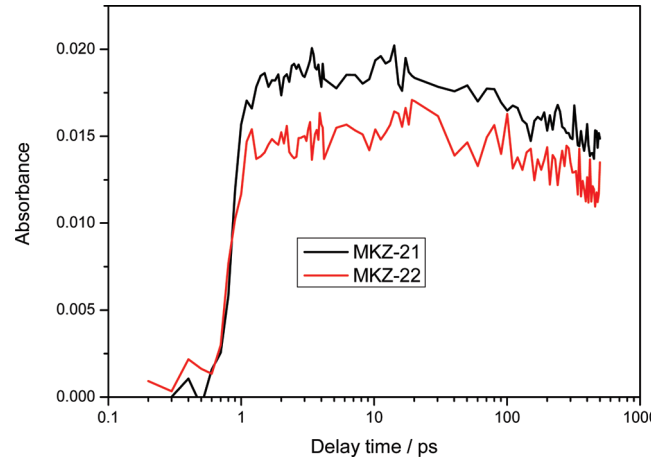

Figure 4. Time profiles of the transient absorption obtained for **MKZ-21** and **MKZ-22** loaded TiO_2 films.

can be defined, are tabulated in Table S1 (Supporting Information). For both the acid and the lithium salt, the angles formed between the indolo[3,2,-*b*]carbazole plane and the first connecting thiophene plane are computed to be 25° and 27° in **MKZ-21** and **MKZ-22**, respectively. Because of the substitution of *n*-hexyl groups, the oligothiophene units are not coplanar with each other, with the torsion angles of around 20°, which may help inhibit the close intermolecular $\pi-\pi$ stacking.[19,36,37] However, the cyanoacrylic acid (cyanoacrylate) group is found to be coplanar with respect to the connecting thiophene unit, indicating the strong conjugation through the thiophene-cyanoacrylic acid (cyanoacrylate) groups.

The calculated molecular orbital energy diagram along with the electron distribution of the frontier molecular orbitals for **MKZ-21** and **MKZ-22** and their lithium salts are shown in Figure 3. Calculated results indicate that the HOMOs and LUMOs of the two sensitizers are all destabilized by about 0.1−0.3 eV from the acid type to the lithium salt mainly because of the frontier obitals destabilization taking place in salt form. The HOMO−LUMO gaps of **MKZ-22**, both in the acid type and in the lithium salt, are a little smaller than those of **MKZ-21** because of the increased π-conjugation. In the above two sensitizers, the HOMOs are primarily comprised of the indolo[3,2,-*b*]carbazole moiety, with little contributions from the oligothiophene units and the anchoring cyanoacrylic acid (cyanoacrylate) group, while the LUMOs are very clearly located through the oligothiophene units and the anchoring cyanoacrylic acid (cyanoacrylate) group, which shows a very obvious electron density shift from the indolo[3,2,-*b*]carbazole core to the cyanoacrylic acid (cyanoacrylate) group upon excitation, allowing an efficient photoinduced electron transfer from the sensitizer to the conduction band of TiO_2 via the anchoring carboxyl group.

We also performed TD-DFT excited states calculations at the B3LYP/6-31G(d) level, given the negligible effect of the solvent, to get insight into the excited states of the above indolo[3,2,-*b*]carbazole based sensitizers at the molecular level. The calculated lowest energies, oscillator strengths (*f*), and compositions in terms of molecular orbital contributions are presented in Table 2. The lowest transitions of all the sensitizers correspond to a charge transfer excitation mainly from the HOMO (indolo[3,2,-*b*]carbazole moieties) to the LUMO (cyanoacrylic acid (cyanoacrylate) groups), as reflected by the electron distribution of the frontier molecular orbitals (Table 2 and Figure 3). Compared with the experimental measurements, the calculated absorption maxima of the two sensitizers are considerably red-shifted (Table 2), which is related to the extended charge-transfer character of this transition, and it could not be properly captured by TD-DFT calculations employing current exchange-correlation functions.[38,39] Similar to the experimental measurements, the calculated absorption maxima of the salt form of the two sensitizers both exhibit blue shift compared with those of the acid type owing to the weak electron acceptor ability of the cyanoacrylate group. The calculated

TABLE 2: Calculated Lowest Excited Energies (eV, nm), Oscillator Strengths (*f*), and Compositions in Terms of Molecular Orbital Contributions, As Compared with the Experimental Absorption Maxima

sensitizer	*E*/eV, nm	*f*	composition[a]	exp/eV, nm
MK-1 (acid)	2.26 (548)	1.00	H-0→L+0(+86%)	2.52 (492)[b]
(Lithium salt)	2.40 (516)	1.16	H-0→L+0(+85%)	2.90 (428)[c]
MKZ-21 (acid)	2.19 (566)	0.56	H-0→L+0(+92%)	2.52 (492)[b]
(Lithium salt)	2.38 (520)	0.73	H-0→L+0(+91%)	2.89 (429)[c]
MKZ-22 (acid)	2.07 (598)	0.67	H-0→L+0(+93%)	2.48 (501)[b]
(Lithium salt)	2.26 (548)	0.92	H-0→L+0(+91%)	2.84 (437)[c]

[a] H means HOMO, and L means LUMO. [b] The maximal absorption in toluene solution. [c] The maximal absorption on TiO_2 film (transparent layer, ~20 nm nanoparticles, 1.5 μm in thickness).

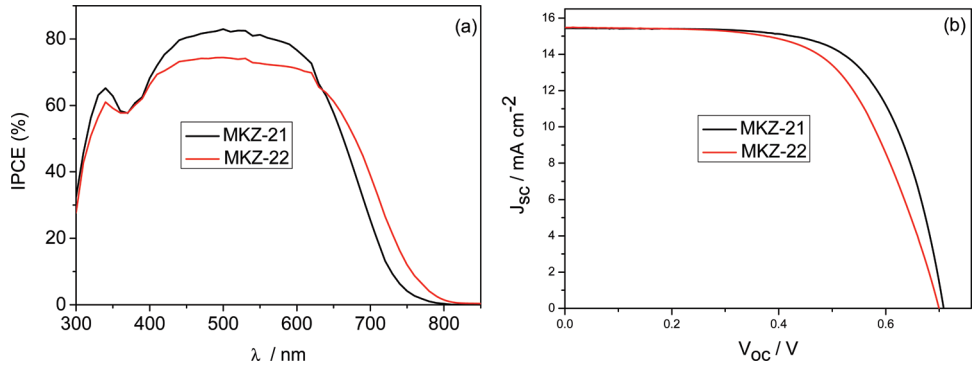

Figure 5. IPCE (a) and $I-V$ curves (b) of DSSCs based on **MKZ-21** and **MKZ-22**.

absorption maximum of **MKZ-22**, not only in acid type but also in lithium salt, is red-shifted as compared with that of **MKZ-21** due to the extended π-conjugation. As expected, the calculated lowest transitions of **MK-1**, both in acid type and in lithium salt, are considerably blue-shifted compared with those of **MKZ-21** and **MKZ-22** (Table 2), which proved our expectation that indolo[3,2-*b*]carbazole unit has stronger electron donating ability than carbazole unit when connected into the similar donor-π-acceptor structure. We speculate that this is the main reason for the following broader IPCE spectra of **MKZ-21** and **MKZ-22** sensitized solar cells than that of **MK-1** sensitized solar cell (Figure S4, Supporting Information).

Femtosecond Transient Absorption. Figure 4 shows the transient absorption kinetics monitored at 3440 nm for **MKZ-21** and **MKZ-22** loaded TiO_2 films covered with electrolyte 3 under excitation at 525 nm. The value of absorbance (0.022) corresponds to the 100% electron injection yield, which was estimated from the transient absorption data of a dye, **N3**: *cis*-bis(thiocyanato)bis(2,2′-bipyridyl-4,4′-dicarboxylic acid)ruthenium(II), loaded TiO_2 film, whose electron injection yield from the excited sensitizer to TiO_2 is 100%.[40,41] Because of electrons injected into the conduction band of TiO_2, the transient absorption for two films increased after photoexcitation of sensitizers. The difference of the transient absorbance between **MKZ-21** and **MKZ-22** loaded films after 1 ps was obviously observed, indicating the different electron injection yields. On the basis of the electron injection yield of the **N3** dye as a reference, the electron injection efficiency was derived from the absolute absorbance at ~100 ps. The electron injection yield from **MKZ-21** to TiO_2 was estimated to be around 75%, and that from **MKZ-22** to TiO_2 was around 65%. The higher electron injection yield of **MKZ-21** than that of **MKZ-22** can be attributed to the corresponding higher excited state oxidation potential of **MKZ-21** compared with **MKZ-22** (Table 1 and Figure 3), which could enhance the driving force of the electron injection from the excited sensitizers to the conduction band of TiO_2. The gradual signal decay observed after 100 ps may be due to the back electron transfer to dye cations or relaxation of electrons in the conduction band; however, the former is unlikely judging from IPCE values obtained in the next section.

Photovoltaic Performance. All of the sensitizers have been used to manufacture solar cell devices to explore current−voltage characteristics using electrolyte 1 or 2. For comparison of the light harvesting ability of **MKZ-21**, **MKZ-22**, and **MK-1**, DSSCs based on dye-sensitized transparent TiO_2 (6 μm) films and electrolyte 1 were used at first, the IPCE spectra are shown in Figure S4, while Figure 5a shows the optimized IPCEs for DSSCs based on **MKZ-21** and **MKZ-22** using 14 μm TiO_2 films and electrolyte 2. IPCE is defined as the number of electrons generated by light in the external circuit divided by the number of incident photons and is presented by the following eq 1, where J_{sc} is the short-circuit photocurrent density, λ is the excitation wavelength, and P_{in} is the incident light intensity.

$$\mathrm{IPCE}(\%) = \frac{1240 J_{sc}(\mu\mathrm{A\ cm^{-2}})}{\lambda(\mathrm{nm}) P_{in}(\mathrm{W\ m^{-2}})} \quad (1)$$

Although DSSCs based on **MKZ-21** and **MK-1** produced similar maximum IPCE in the spectra range of 350−600 nm, the onset of the IPCE spectra of both **MKZ-21** and **MKZ-22** sensitized solar cells is more red-shifted than that of **MK-1** sensitized solar cell (Figure S4), consisting with both the absorption measurements and the theoretical calculations. The broadening of the IPCE spectra is prerequisite for a larger photocurrent and a higher conversion efficiency, indicating the promising application of the sensitizers based on indolo[3,2-*b*]carbazole unit in DSSCs.

The optimized IPCE data of **MKZ-21** and **MKZ-22** sensitized solar cells plotted as a function of excitation wavelength exhibit a plateau higher than 70% in the range from 420 to 620 nm with a maximal value of 83% at 500 nm for the DSSC based on **MKZ-21**. Considering the reflection and absorption losses in the transparent conducting oxide (TCO) substrate, the net photon-to-current conversion efficiency in this range would exceed 90%, which indicates the highly efficient performance of the solar cells based on indolo[3,2-*b*]carbazole sensitizers. The onset of the IPCE spectrum of **MKZ-22** sensitized solar cell is red-shifted by about 30 nm as compared with **MKZ-21** as a result of the extended π-conjugation, being consistent with the UV−vis absorption spectra of the dye-loaded TiO_2 films (Figure 2b). However, the lower maximum IPCE of the DSSC based on **MKZ-22** was observed than that of **MKZ-21**, which could be explained by the result of the transient absorption spectroscopy measurements that the electron injection yield of **MKZ-22** was relatively lower than that of **MKZ-21**, as shown in Figure 4.

Figure 5b presents the optimized $J-V$ curves of the solar cells based on **MKZ-21** and **MKZ-22** using 14 μm TiO_2 films and electrolyte 2. The relations between these photovoltaic parameters are as follows, where P_{in} is the intensity of the incident light and P_{max} is the power output maximum of the solar cell.

$$\eta = \frac{J_{sc} V_{oc} FF}{P_{in}}, \quad FF = \frac{P_{max}}{J_{sc} V_{oc}} \quad (2)$$

Under AM 1.5G irradiation (100 mW cm^{-2}), the **MKZ-21** sensitized solar cell gave a short-circuit photocurrent density

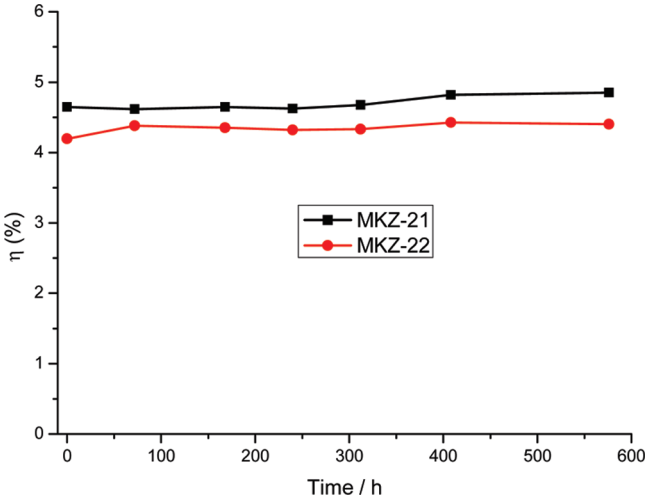

Figure 6. Variations of the conversion efficiency of the solar cells sensitized with **MKZ-21** and **MKZ-22** during long time visible-light irradiation.

(J_{sc}) of 15.4 mA cm^{-2}, an open-circuit voltage (V_{oc}) of 0.71 V, and a fill factor (*FF*) of 0.67, corresponding to an overall conversion efficiency (η) of 7.3%. While under the same conditions, the **MKZ-22** sensitized solar cell gave a J_{sc} of 15.5 mA cm^{-2}, a V_{oc} of 0.70 V, and a *FF* of 0.62, corresponding to a η of 6.7%. The slightly larger J_{sc} of the **MKZ-22** sensitized solar cell as compared with that of a solar cell based on **MKZ-21** demonstrates the beneficial influence of the red-shifted absorption spectrum of **MKZ-22** on TiO_2 film and the broadening of the IPCE spectrum of **MKZ-22** sensitized solar cell. However, the lower *FF* of **MKZ-22** sensitized solar cell, due to the larger molecular size of **MKZ-22** than that of **MKZ-21**,[19] finally led to the lower conversion efficiency of **MKZ-22** sensitized solar cell.

Figure 6 shows the variations of the conversion efficiency of solar cells sensitized with **MKZ-21** and **MKZ-22** under continuous visible-light irradiation (AM 1.5G, 100 mW cm^{-2}) with a UV (<420 nm) cutoff filter, using transparent TiO_2 (6 μm, ~20 nm nanoparticles) films and electrolyte 3. No degradation of the solar cell performances of the DSSCs based on **MKZ-21** and **MKZ-22** was observed under white-light irradiation at 50 °C. In the preliminary experiment, the values of the overall conversion efficiency (η) were recorded over a period of near 600 h. As a result, the solar cell performances of DSSCs based on both dyes still retained as an initial efficiency after 600 h under light irradiation. The remarkable stability of dyes, **MKZ-21** and **MKZ-22**, can be attributed to the hydrophobic long *n*-octyl and *n*-hexyl aliphatic chains, which could prevent water induced dye desorption from the TiO_2 surface.

Conclusions

Two new organic sensitizers **MKZ-21** and **MKZ-22**, based on indolo[3,2,-*b*]carbazole unit, were synthesized and used for sensitizing TiO_2 electrodes for the first time, yielding a good performance with 83% IPCE and 7.3% overall conversion efficiency under standard AM 1.5G irradiation (100 mW cm^{-2}). Both of the solar cells based on **MKZ-21** and **MKZ-22** and fabricated using an electrolyte in MPN exhibited good stability under a long time visible-light irradiation. When connected into the similar donor-π-acceptor structure, the electron donating ability of indolo[3,2-*b*]carbazole unit is stronger than that of carbazole unit. Our results strongly indicate that the application of indolo[3,2-*b*]carbazole based sensitizers in DSSCs is promising.

Increasing the number of the thiophene units can extend the π-conjugation and increase the short-circuit photocurrent as the result of the red-shifted absorption of the sensitizer loaded TiO_2 film. But at same time, increasing the number of thiophene units can also make the LUMO energy level of the sensitizer lower, which could give lower electron injection yield. In an effort to obtain the improved performance of the DSSCs based on indolo[3,2,-*b*]carbazole sensitizers, further structural modification of the sensitizers for tuning the frontier orbital energy, the optimization of the solar cell devices, and some measurements of the kinetic processes are in progress.

Acknowledgment. We acknowledge financial support from the New Energy and Industrial Technology Development Organization (NEDO) of Japan.

Supporting Information Available: Molecular structure of **MK-1**; synthesis procedures and characterization of **MKZ-21** and **MKZ-22**; optimized ground-state geometries, atom labels, dihedral angles from the optimized structures, the calculated molecular orbital energy diagrams and isodensity surface plots of the HOMOs and LUMOs for **MKZ-21**, **MKZ-21**, and **MK-1**; IPCE curves of the DSSCs based on **MKZ-21**, **MKZ-22**, and **MK-1** using transparent TiO_2 (6 μm) films and electrolyte 1. This material is available free of charge via the Internet at http://pubs.acs.org.

References and Notes

(1) O'Regan, B.; Grätzel, M. *Nature* **1991**, *353*, 737.
(2) Nazeeruddin, M. K.; Kay, A.; Rodicio, I.; Humphry-Baker, R.; Müller, E.; Liska, P.; Vlachopoulos, N.; Grätzel, M. *J. Am. Chem. Soc.* **1993**, *115*, 6382.
(3) Nazeeruddin, M. K.; Péchy, P.; Renouard, T.; Zakeeruddin, S. M.; Humphry-Baker, R.; Comte, P.; Liska, P.; Cevey, L.; Costa, E.; Shklover, V.; Spiccia, L.; Deacon, G. B.; Bignozzi, C. A.; Grätzel, M. *J. Am. Chem. Soc.* **2001**, *123*, 1613.
(4) Grätzel, M. J. *Photochem. Photobiol. A* **2004**, *164*, 3.
(5) Nazeeruddin, M. K.; Angelis, F. D.; Fantacci, S.; Selloni, A.; Viscardi, G.; Liska, P.; Ito, S.; Takeru, B.; Grätzel, M. *J. Am. Chem. Soc.* **2005**, *127*, 16835.
(6) Wang, Z.-S.; Li, F.-Y.; Huang, C.-H.; Wang, L.; Wei, M.; Jin, L.-P.; Li, N.-Q. *J. Phys. Chem. B* **2000**, *104*, 9676.
(7) Hara, K.; Kurashige, M.; Dan-oh, Y.; Kasada, C.; Shinpo, A.; Suga, S.; Sayama, K.; Arakawa, H. *New J. Chem.* **2003**, *27*, 783.
(8) Hara, K.; Sato, T.; Katoh, R.; Furube, A.; Ohga, Y.; Shinpo, A.; Suga, S.; Sayama, K.; Sugihara, H.; Arakawa, H. *J. Phys. Chem. B* **2003**, *107*, 597.
(9) Horiuchi, T.; Miura, H.; Sumioka, K.; Uchida, S. *J. Am. Chem. Soc.* **2004**, *126*, 12218.
(10) Kitamura, T.; Ikeda, M.; Shigaki, K.; Inoue, T.; Anderson, N. A.; Ai, X.; Lian, T.; Yanagida, S. *Chem. Mater.* **2004**, *16*, 1806.
(11) Li, C.; Wang, W.-B.; Wang, X.-S.; Zhang, B.-W.; Cao, Y. *Chem. Lett.* **2005**, *34*, 554.
(12) Hara, K.; Sato, T.; Katoh, R.; Furube, A.; Yoshihara, T.; Murai, M.; Kurashige, M.; Ito, S.; Shinpo, A.; Suga, S.; Arakawa, H. *Adv. Funct. Mater.* **2005**, *15*, 246.
(13) Ito, S.; Zakeeruddin, S. M.; Humphry-Baker, R.; Liska, P.; Charvet, R.; Comte, P.; Nazeeruddin, M. K.; Péchy, P.; Takata, M.; Miura, H.; Uchida, S.; Grätzel, M. *Adv. Mater.* **2006**, *18*, 1202.
(14) Koumura, N.; Wang, Z.-S.; Mori, S.; Miyashita, M.; Suzuki, E.; Hara, K. *J. Am. Chem. Soc.* **2006**, *128*, 14256. (Addition and Correction **2008**, *130*, 4202).
(15) Kim, S.; Lee, J. K.; Kang, S. O.; Ko, J.; Yum, J.-H.; Fantacci, S.; De Angelis, F.; Di Censo, D.; Nazeeruddin, M. K.; Grätzel, M. *J. Am. Chem. Soc.* **2006**, *128*, 16701.
(16) Zhang, X.-H.; Li, C.; Wang, W.-B.; Cheng, X.-X.; Wang, X.-S.; Zhang, B.-W. *J. Mater. Chem.* **2007**, *17*, 642.
(17) Wang, Z.-S.; Cui, Y.; Dan-oh, Y.; Kasada, C.; Shinpo, A.; Hara, K. *Adv. Mater.* **2007**, *19*, 1138.
(18) Hagberg, D. P.; Yun, J.-H.; Lee, J. K.; Angelis, F. D.; Marinado, T.; Karlsson, K. M.; Humphry-Baker, R.; Sun, L.-C.; Hagfeldt, A.; Grätzel, M.; Nazeeruddin, M. K. *J. Am. Chem. Soc.* **2008**, *130*, 6259.
(19) Wang, Z.-S.; Koumura, N.; Cui, Y.; Takahashi, M.; Sekiguchi, H.; Mori, A.; Kubo, T.; Furube, A.; Hara, K. *Chem. Mater.* **2008**, *20*, 3993.

(20) Qin, H.; Wenger, S.; Xu, M.-F.; Gao, F.-F.; Jing, X.-Y.; Wang, P.; Zakeeruddin, S. M.; Grätzel, M. *J. Am. Chem. Soc.* **2008**, *130*, 9202.
(21) Hu, N.-X.; Xie, S.; Popovic, Z.; Ong, B.; Hor, A.-M. *J. Am. Chem. Soc.* **1999**, *121*, 5097.
(22) Wakim, S.; Bouchard, J.; Simard, M.; Drolet, N.; Tao, Y.; Leclerc, M. *Chem. Mater.* **2004**, *16*, 4386.
(23) Li, Y.; Wu, Y.; Gardner, S.; Ong, B. S. *Adv. Mater.* **2005**, *17*, 849.
(24) Wu, Y.; Li, Y.; Gardner, S.; Ong, B. S. *J. Am. Chem. Soc.* **2005**, *127*, 614.
(25) Li, Y.; Wu, Y.; Ong, B. S. *Macromolecules* **2006**, *39*, 6521.
(26) Belletête, M.; Blouin, N.; Boudreault, P.-L. T.; Leclerc, M.; Durocher, G. *J. Phys. Chem. A* **2006**, *110*, 13696.
(27) Boudreault, P.-L. T.; Wakim, S.; Blouin, N.; Simard, M.; Tessier, C.; Tao, Y.; Leclerc, M. *J. Am. Chem. Soc.* **2007**, *129*, 9125.
(28) Wang, P.; Zakeeruddin, S. M.; Moser, J. E.; Nazeeruddin, M. K.; Sekiguchi, T.; Grätzel, M. *Nat. Mater.* **2003**, *2*, 402.
(29) Wang, P.; Zakeeruddin, S. M.; Comte, P.; Charvet, R.; Humphry-Baker, R.; Grätzel, M. *J. Phys. Chem. B* **2003**, *107*, 14336.
(30) Chio, H.; Baik, C.; Kang, S. O.; Ko, J.; Kang, M.-S.; Nazeeruddin, M. K.; Grätzel, M. *Angew. Chem., Int. Ed.* **2008**, *47*, 327.
(31) Frisch, M. J.; Trucks, G. W.; Schlegel, H. B.; Scuseria, G. E.; Robb, M. A.; Cheeseman, J. R.; Montgomery, J. A.; Jr.; Vreven, T.; Kudin, K. N.; Burant, J. C.; Millam, J. M.; Iyengar, S. S.; Tomasi, J.; Barone, V.; Mennucci, B.; Cossi, M.; Scalmani, G.; Rega, N.; Petersson, G. A.; Nakatsuji, H.; Hada, M.; Ehara, M.; Toyota, K.; Fukuda, R.; Hasegawa, J.; Ishida, M.; Nakajima, T.; Honda, Y.; Kitao, O.; Nakai, H.; Klene, M.; Li, X.; Knox, J. E.; Hratchian, H. P.; Cross, J. B.; Bakken, V.; Adamo, C.; Jaramillo, J.; Gomperts, R.; Stratmann, R. E.; Yazyev, O.; Austin, A. J.; Cammi, R.; Pomelli, C.; Ochterski, J. W.; Ayala, P. Y.; Morokuma, K.; Voth, G. A.; Salvador, P. J.; Dannenberg, J.; Zakrzewski, V. G.; Dapprich, S.; Daniels, A. D.; Strain, M. C.; Farkas, O.; Malick, D. K.; Rabuck, A. D.; Raghavachari, K.; Foresman, J. B.; Ortiz, J. V.; Cui, Q.; Baboul, A. G.; Clifford, S.; Cioslowski, J.; Stefanov, B. B.; Liu, G.; Liashenko, A.; Piskorz, P.; Komaromi, I.; Martin, R. L.; Fox, D. J.; Keith, T.; Al-Laham, M. A.; Peng, C. Y.; Nanayakkara, A.; Challacombe, M.; Gill, P. M. W.; Johnson, B.; Chen, W.; Wong, M. W.; Gonzalez, C.; Pople, J. A. *Gaussian 03, Revision D.01*, Gaussian, Inc., Wallingford CT, 2004.
(32) (a) Becke, A. D. *J. Chem. Phys.* **1993**, *98*, 5648. (b) Lee, C.; Yang, W.; Parr, R. G. *Phys. Rev. B* **1988**, *37*, 785.
(33) Furube, A.; Katoh, R.; Hara, K.; Sato, T.; Murata, S.; Arakawa, H.; Tachiya, M. *J. Phys. Chem. B* **2005**, *109*, 16406.
(34) Wang, Z.-S.; Kawauchi, H.; Kashima, T.; Arakawa, H. *Coord. Chem. Rev.* **2004**, *248*, 1381.
(35) Hagfeldt, A.; Grätzel, M. *Chem. Rev.* **1995**, *95*, 49.
(36) Azumi, R.; Götz, G.; Debaerdemaeker, T.; Bäuerle, P. *Chem.—Eur. J.* **2000**, *6*, 735.
(37) Kiriy, N.; Kiriy, A.; Bocharova, V.; Stamm, M.; Richter, S.; Plötner, M.; Fischer, W.-J.; Krebs, F. C.; Senkovska, I.; Adler, H.-J. *Chem. Mater.* **2004**, *16*, 4757.
(38) Dreuw, A.; Head-Gordon, M. *J. Am. Chem. Soc.* **2004**, *126*, 4007.
(39) Tozer, D. J.; Amos, R. D.; Handy, N. C.; Roos, B. O.; Serrano-Andres, L. *Mol. Phys.* **1999**, *97*, 859.
(40) Katoh, R.; Furube, A.; Yoshihara, T.; Hara, K.; Fujihashi, G.; Takano, S.; Murata, S.; Arakawa, H.; Tachiya, M. *J. Phys. Chem. B* **2004**, *108*, 4818.
(41) Furube, A.; Du, L.; Hara, K.; Katoh, R.; Tachiya, M. *J. Am. Chem. Soc.* **2007**, *129*, 14852.

JP808536V